A high sensitivity and multi-axis fringing electric field based capacitive tactile force sensor for robot assisted surgery

A high sensitivity and multi-axis fringing electric field based capacitive tactile force sensor for robot assisted surgery

Adeel Arshad [a], Muhammad Mubasher Saleem[a,b,*], Mohsin Islam Tiwana[a,b], Hamood ur Rahman[c], Sohail Iqbal[d] and Rebecca Cheung[e]

[a] Department of Mechatronics Engineering, National University of Sciences and Technology, Islamabad 44000, Pakistan

[b] National Centre of Robotics and Automation (NCRA), Islamabad 44000, Pakistan

[c] Research Directorate, National University of Sciences and Technology, Islamabad 44000, Pakistan

[d] Department of Mechanical and Aerospace Engineering, Air University, Islamabad 44000, Pakistan

[e] Institute for Integrated Micro and Nano Systems, School of Engineering, University of Edinburgh, Scottish Microelectronics Centre, Edinburgh EH9 3FF, UK

* Correspondence: mubasher.saleem@ceme.nust.edu.pk

Keywords:
Multi-axis force sensor
Tactile sensor
Fringing electric field
Elastomer
Rapid prototyping
Robotic surgery

Abstract

This paper presents a design of multi-axis tactile force sensor using the fringe effect of an electric field between stationary patterned electrodes. The unique configuration of the electrodes consisting of four separate square-shaped sensing electrodes, with each encircled by excitation electrodes, allows to achieve enhanced fringe field effect and hence sensitivity. The proposed sensor can decouple the normal, shear and angular shear applied forces. The sensor is fabricated using low-cost rapid prototyping techniques with flexible Ecoflex 00-30 and silicone rubber RTV-528 as the elastomers for contact with the environment. An analytical model is developed that correlates the nominal capacitance of the sensor with that of the geometric dimensions of the stationary electrodes and air cavity height between the electrodes and elastomer. The force measurement ranges in the normal, shear, and angular axis are 5 N, 1.5 N, and 1 N respectively. The sensor shows a perfectly linear response, repeatability,and a low hysteresis error, thermal stability and robustness to the environmental interferances that makes it suitable to be used for force feedback in minimally invasive robotic surgery.

1. Introduction

In minimally invasive robotic surgery (MIRS), a surgeon can perform internal body inspection through small skin incisions with surgical instruments. This method reduces hospitalization time, postoperative infection, anesthesia time, incision size, trauma, and intraoperative blood loss [1]. Despite these advantages, there are also some limitations for surgeons in MIRS such as the loss of kinesthetic (force) and cutaneous (tactile) feedback [2], which affects the surgical efficacy and efficiency of the medical treatment [3]. To overcome this problem, tactile force sensors are used with surgical instruments in MIRS which provide cutaneous and kinesthetic feedback to surgeons. These sensors provide surgeons with the necessary feedback to avoid the application of excessive force and thus reduce the risk of tissue damage. With the recent technological advancements in the domain of robotics, tactile sensors have become an emerging topic due to their vast application in the robotics, and medical fields [4]. The attributes provided by tactile sensors showed their functionality in many applications, such as in the evolution of efficient object manipulation tasks [5, 6], and safe human-machine interaction [7, 8]. Currently, tactile force sensors have been developed for multi-axis force detection using different transduction mechanisms including piezoelectric [9, 10], piezoresistive [11,12], inductive [13,14], magnetic [15,16], and capacitive [17,18]. Piezoelectric force sensors utilize the piezoelectric effect of ceramic elements and quartz crystal effect for the detection of force with high stability and linearity [19]. However, piezoelectric sensors are only capable of detecting dynamic forces and require recalibration with time [20]. Piezoresistive force sensors utilize the effect of resistance change in materials, due to input force and have the advantages of relatively easy fabrication and simple readout electronics [21, 22]. However, in many applications, piezoresistive sensors are not suitable due to their poor output consistency and temperature sensitivity [23]. Inductive force sensors work on the principle of Faraday's law of induction to measure the force and have a high sensitivity along with a wide measurement range [24, 25]. However, such sensors have a poor dynamic response and long-term reliability.

Capacitive tactile force sensors have many advantages over other transduction mechanisms due to their high sensitivity, long-time stability, durability, and adaptability to the environment [26]. In previous studies, different types of capacitive sensors were proposed based on comb structures [27], overlapping parallel plates [28], and in-plane electrodes utilizing the fringing field effect [29]. The capacitive force sensors with an overlapping area, are based on the capacitance change due to a change in gap between two overlapping plates under an applied force [30, 31]. These overlapping capacitive sensors have low sensitivity such as Fernandes et al. [32] proposed a multi-axis capacitive sensor for normal, shear, and angular force detection with a high range but the main drawback of the sensor is low sensitivity for both the normal and shear applied forces. In comparison to the overlapping area-based capacitive force sensors, fringing field-effect based capacitive

sensors allow avoiding the parallel plate electrodes alignment errors, to achieve linear output response and physically isolated from the sensing environment. The working of such capacitive force sensors is based on the concept of change in capacitance due to changes in the effective dielectric medium above the capacitive plates under an applied force. Huang et al. [29] presented a fringing field effect based tri-axial tactile force sensor with four sensing electrodes and one public electrode. The sensor measures the normal and shear force for a force range of 0-10 N with the sensitivity of 0.0095/N, 0.0053/N, and 0.006/N for normal, shear *x*-axis and *y*-axis. However, the configuration of the electrodes on the fixed substrate does not allow measuring the angular shear force. Sun et al. [33] presented a fringing field effect-based tactile force sensor with four comb-type sensing electrodes and one public electrode with normal and shear forces measurement range of 0-10 N. The output response of the sensor is linear in the range of 0-5 N only and nonlinearity increases exponentially for an applied force up to 10 N. In this paper, a low-cost, and multi-axis fringing field effect based capacitive tactile force sensor design is presented with a unique configuration of the electrodes on the substrate to achieve enhanced fringing electric field effect and hence sensitivity. The proposed sensor design can measure angular shear forces in addition to both the normal and shear *xy*-axis forces.

2. Sensor Design and Working Principle

Figure. 1 (a) and (b) show an exploded and cross-sectional view of the proposed multi-axis fringing electric field effect based capacitive tactile force sensor respectively. The top layer of the sensor is octagonal shaped elastomer silicone rubber (RTV-528) bump which is encapsulated with a 3D printed Polylactic acid (PLA) based dome. The octagonal-shaped top elastomer (RTV-528) and dome allow applying the force uniformly in different directions on the sensor. The second part of the sensor is a dual-layer structure that consists of an air cavity and an elastomer Ecoflex 00-30 on the top. The elastomer dome used in the design is silicone rubber (RTV-528) with a higher Young's modulus in comparison to the Ecoflex 00-30 which results in maximum force transfer to the Ecoflex 00-30. The third and last layer of the sensor consists of four sensing electrodes surrounded by four excitation electrodes. One excitation and one sensing electrode make a one-unit capacitor. The enhanced fringing electric field effect is achieved by increasing the length of an electrode in the minimum area by using a unique pattern of electrodes. These electrodes are patterned on the FR4 printed circuit board (PCB) and form four-unit capacitors (C_1- C_4) as shown in Fig. 1(c). The elastomer Ecoflex 00-30 and the air cavity above the electrodes act as a dielectric material for the four-unit capacitors. The total area of a unit capacitor is 3.25 mm × 3.25 mm with an inner electrode area of 1.5 mm × 1.5 mm. The outer electrode width is 0.75 mm and is placed at a distance of 0.125 mm from the inner electrode. The size of air cavity between the elastomer Ecoflex 00-30 and a unit capacitor on the substrate is 1.2 mm. The overall sensor size is 12 mm × 12 mm × 14 mm. The sensor is designed to be attached at the root of a surgical tool, integrated at the end of a robotic surgical arm, as shown in Fig. 1(d). The surgical tool is to be fixed exactly at the center of the tactile force sensor such that the normal force applied to the sensor through surgical tool uniformly deforms the sensor surface downwards.

Figure 2 (a) shows the 3D schematic of the sensor with direction of forces applied in normal, ±*xy*-shear axis and at an angle. When a normal force is applied to the top elastomer dome, the Ecoflex 00-30 elastomer moves downwards (-*z*-axis), and the air cavity gap decreases as shown in Fig. 2 (b) and (c). For an applied normal force, the dielectric medium above the capacitor units changes from air to Ecoflex 00-30 which has a higher dielectric constant ($\varepsilon_e = 2.8$) then the air ($\varepsilon_0 = 1$). Thus, the dielectric constant value for the proposed sensor lies in the range of 1 to 2.8 for an applied normal force. For an applied shear force, the bending of the elastomer Ecoflex 00-30 results in an increase in the air cavity thickness on the side where forces are applied and a decrease on the opposite side as shown in Fig. 2 (d). For an applied shear force in the +*x* direction, the bending of the elastomer results in a decrease in capacitance in the capacitor units C_1, and C_2 and an increase in capacitance in the capacitor units C_3, C_4 due to a change in the effective dielectric constant. For the proposed sensor, the size of electrodes remains constant with the application of a force, however, the structure of the multi-layered dielectric changes, which leads to a change in the effective dielectric constant which results in a capacitance change in the capacitor units. Figure 3(a) and (b) show the electric field lines distribution and corresponding electric field strength with the downwards displacement of the elastomer, before and after an applied normal force. The electric field strength increases as the dielectric air medium above the capacitor units is replaced with the elastomer medium of higher dielectric constant for an applied force. Moreover, under an applied force, the electric field lines are concentrated in the region above capacitor unit electrodes. This leads to a higher value of output capacitance of a capacitor unit. The layout of the capacitor units for the sensor allows to fully decouple the forces applied in normal, shear, and angular directions. Table. 1 shows the complete sensing scheme for the proposed sensor for an applied force in different axes. The upwards arrow (↑), downwards arrow (↓) and dot (•) symbols represent increase, decrease and no change in capacitance values respectively. For example, for an applied normal force, the capacitance in the all four capacitor units increases and for an applied +*x*-axis shear force, the capacitance of the capacitor unit C_1 and C_2 decreases while that of C_3 and C_4 increases. The output capacitance change for the four capacitor units is unique for an input force in the normal, ±*xy*-shear axis and at an angle which allows to fully decouple the input forces applied to the sensor.

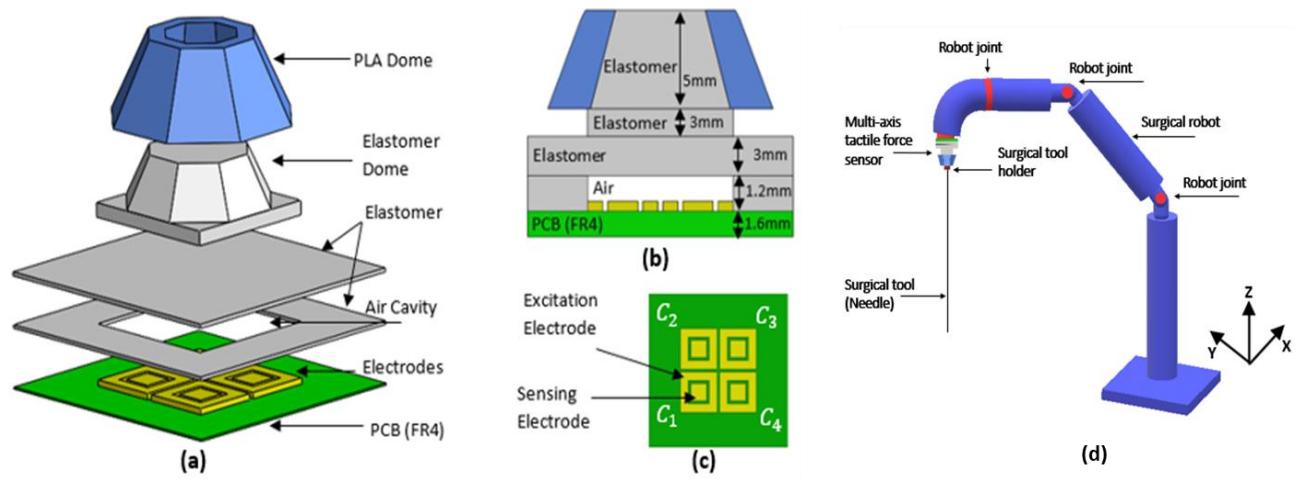

Fig. 1 (a) Exploded view of the sensor (b) cross-sectional view of the sensor (c) sensing and excitation electrodes configuration (d) integration scheme of the sensor with the robotic arm and surgical tool.

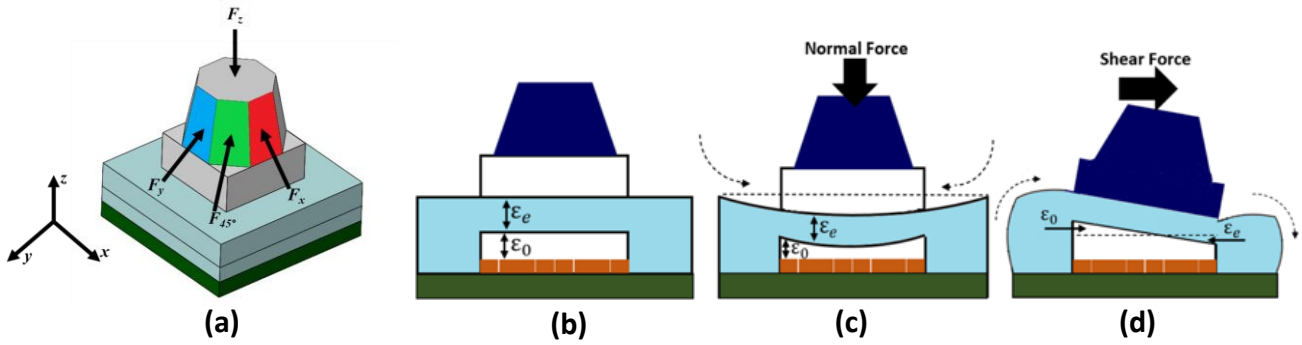

Fig. 2. (a) 3D view of the sensor with applied force direction and cross-sectional view of the sensor under (b) no force (c) normal force (d) shear force

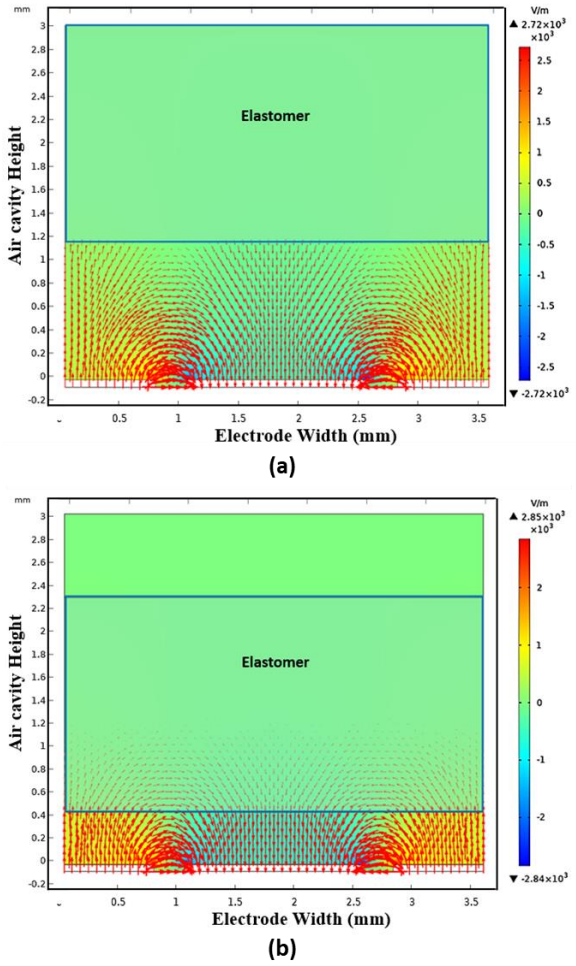

Fig. 3. Electric field strength and field lines distribution with respect to the position of top elastomer (a) no force (b) applied normal force.

The Eq. (1) to (7) show analytical formulation for the force estimation based on the measured capacitance values of the four capacitor units under applied force in different axes.The ΔC_1, ΔC_2, ΔC_3 and ΔC_4 are normalized capacitance change values of the individual capacitor units C_1, C_2, C_3, and C_4 respectively. When a normal force is applied to the sensor then a positive change occurs in all the capacitor units according to Eq. (1). For a shear force in the x-axis, a positive capacitance change occurs in in the capacitor units C_1 and C_2 while a negative change occurs in the capacitors C_3 and C_4. However, in the case of shear force in the y-axis, a positive change occurs in the capacitance of capacitor units C_2 and C_3 as expressed in Eq. (3) while a negative change occurs in the capacitor units C_1 and C_4. In the case of angular shear force in the first quadrant, a positive capacitance change occurs in the capacitor unit C_3, negative change occurs in the C_1 while no change takes place in the capacitance of capacitor units C_2 and C_4.

Table 1. Sensing scheme for the proposed sensor for an applied force in the normal, ±xy-shear axis, and angular axis

Applied Force	Normalized Capacitance Change			
	ΔC_1	ΔC_2	ΔC_3	ΔC_4
Normal	↑	↑	↑	↑
Shear (+x)	↓	↓	↑	↑
Shear (-x)	↑	↑	↓	↓
Shear (+y)	↓	↑	↑	↓
Shear (-y)	↑	↓	↓	↑
Angle (45°)	↓	•	↑	•
Angle (135°)	•	↑	•	↓
Angle (225°)	↑	•	↓	•
Angle (315°)	•	↓	•	↑

In the case of angular shear force in the second quadrant positive change take place in the capacitance of C_4, negative change in C_2 and no change come out in C_1 and C_3. For an angular shear force in the third quadrant, a positive capacitance change occurs in the capacitor unitC_1, a negative change occurs in the C_3, and no change occur in the capacitor units C_2 and C_4. When a shear force is applied in the fourth quadrant, the capacitance of C_2 is increased, the capacitance of C_4 is deceased while the capacitance of C_1 and C_3 remains constant. For an angular force at 45º, the capacitance of the capacitor unit C_1 decreases and C_3 increases while it remains constant for the capacitor units C_2 and C_4.

$$\Delta C_Z = (\Delta C_1 + \Delta C_2 + \Delta C_3 + \Delta C_4) \quad (1)$$

$$\Delta C_X = (\Delta C_3 + \Delta C_4) - (\Delta C_1 + \Delta C_2) \quad (2)$$

$$\Delta C_Y = (\Delta C_2 + \Delta C_3) - (\Delta C_1 + \Delta C_4) \quad (3)$$

$$\Delta C_{45^\circ} = \Delta C_3 - \Delta C_1 + (\Delta C_2 + \Delta C_4) \quad (4)$$

$$\Delta C_{135^\circ} = \Delta C_2 - \Delta C_4 + (\Delta C_2 + \Delta C_4) \quad (5)$$

$$\Delta C_{225^\circ} = \Delta C_1 - \Delta C_3 + (\Delta C_2 + \Delta C_4) \quad (6)$$

$$\Delta C_{315^\circ} = \Delta C_4 - \Delta C_2 + (\Delta C_1 + \Delta C_3) \quad (7)$$

3. Sensor Fabrication

Figure. 4 shows the fabrication process steps for the proposed multi-axis capacitive tactile force sensor. In the first step, the elastomers are prepared for the top dome and dielectric layer using elastomers silicone rubber RTV-528 and Ecoflex 00-30 respectively. The elastomers are shaped using PLA-based molds manufactured using 3D printing technology. The silicone rubber RTV-528 elastomer was

mixed with a 1% curing agent by volume and stirred for 3 minutes.

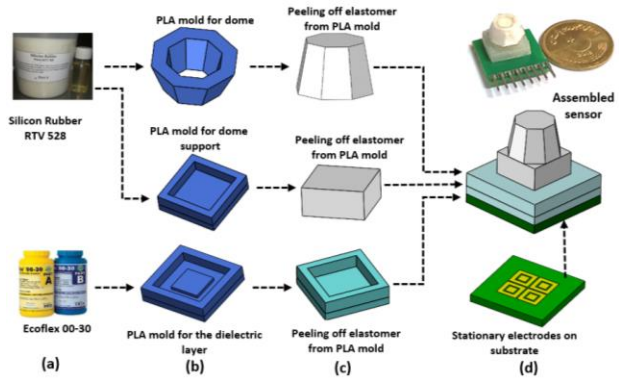

Fig.4. (a) Silicon rubber RTV-528 and Ecoflex 00-30 elastomer (b) PLA molds (c) elastomers (d) assembled sensor with the size reference of a coin.

After stirring thoroughly and degassing, the prepared uncured RTV-528 elastomer was poured into the 3D-printed mold. After curing at room temperature for 24 hours, the cured RTV-528 elastomer layer was peeled off from the 3D-printed molds. The same procedure was used for the Ecoflex 00-30 elastomer with a curing time of 4 hours. The capacitive electrodes are fabricated using conventional technology on an FR4 substrate. The cyanoacrylate glue is used for the final assembling of different parts of the multiaxial force sensor. The assembled multi-axis tactile force sensor is shown in Fig. 4(d). The proposed multi-axis tactile sensor is to be attached with the surgical robot and will not be in direct contact with the internal body organs that resolves the issue of biocompatibility of the material.

4. FEM Modelling

4.1 Nominal Capacitance Model

Li et al. 2014 [34], presented a generic analytical formulation for the nominal capacitance between the two parallel plates lying on the same plane based on the effective theory which is given as;

$$C_o = \eta \times \varepsilon_0 \times b \times \left(\frac{a}{d}\right)^{\frac{2}{\pi}\arctan\left(\frac{d}{b}\right)} X^{\beta} \times Y^{\gamma} \qquad (8)$$

Where $X = (1 + \frac{b}{a})$, $Y = (\frac{d}{a})$, a and b are the width and length of the plates respectively while d refers to in-plane spacing between the plates. The parameters X and Y are electrodes scale dependent while η, β, and γ are geometry-dependent parameters. Since for the proposed tactile force sensor, the geometric configuration of the electrodes is unique where a single sensing electrode is surrounded by an excitation electrode for each capacitor unit instead of simple double plate configuration, therefore values of the η, β, and γ parameters in Eq. 8 is estimated first. For the proposed sensor, the values of η, β, and γ are obtained by modeling three different geometries with different values of electrodes dimensions a, and b (as shown in Table. 2) in COMSOL Multiphysics and performing the nominal capacitance analysis. The nominal capacitance values obtained through analysis for each geometry are used in Eq. (8) to obtain three different equations which are simultaneously solved by using MATLAB's fsolve function which is based on the Trust-region-dogleg optimization algorithm to find the values of η, β, and γ parameters as 41.63, ¬0.64 and 0.0262 respectively which modifies the Eq. (8) as;

$$C_O = 41.63 \times \varepsilon_0 \times b \left(\frac{a}{d}\right)^{\frac{2}{\pi}\arctan\left(\frac{d}{b}\right)} X^{-0.64} \times Y^{0.0262} \qquad (9)$$

The nominal capacitance value obtained from Eq. 9 is compared with the experimentally measured nominal value of capacitor units of the proposed sensor in the absence of top dielectric. The experimental nominal capacitance value of 0.4 pF matches that obtained through Eq. (9) i.e., 0.392 pF.

Table 2. Dimensions of three different geometric configurations of the sensing electrodes.

Geometry	b (mm)	a (mm)	Aspect ratio (b/a)	Area (mm^2)
N_1	1.5	1.5	1	6
N_2	2	1	0.5	6
N_3	2.5	0.75	0.3	6

The limitation of the analytical formulation for the nominal capacitance presented in Eq. (9) for the proposed capacitive tactile force sensor is that it does not consider the effect of air cavity height present between the bottom electrodes and top dielectric layer. To include the effect of air cavity, nominal capacitance analysis is carried out using FEM simulations with varying air cavity sizes and a nonlinear curve fitting is performed on the data curve to obtain the following equation,

$$C_f = C_o \times \varepsilon_r \times 0.05/e^{h^5} + 3.9e^{-13} \qquad (10)$$

Where h represents the air cavity height between the bottom electrodes and top elastomer dielectric layer. This formulation considers the effect of both the geometric configuration of the electrodes for the proposed sensor and air cavity height. The air cavity height above the four capacitor units of the sensor is assumed constant which justified from the FEM based deformation profile of the sensor in response to the normal force, discussed in Section 4.2. Figure 5 shows the comparison of the nominal capacitance values obtained through FEM-based capacitance analysis simulations with that obtained through Eq. (10). The close correspondence between the two shows that Eq. (10) can be used for the analytical

approximation of the nominal capacitance for the proposed capacitive tactile force sensor.

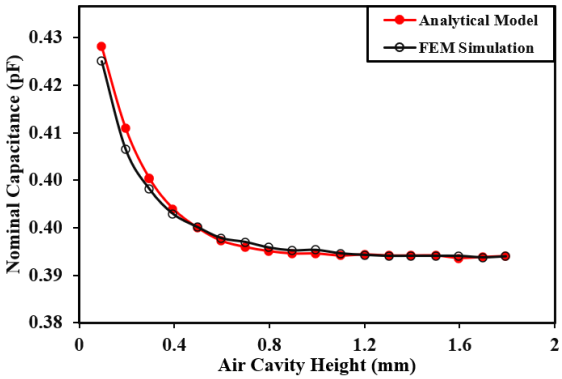

Fig. 5. Comparison of the simulated and calculated nominal capacitance with varying air cavity heights.

4.2 Displacement Analysis Under Applied Force

The working of the sensor under both normal and shear applied forces is verified through FEM simulations. The physical properties of the elastomers presented in [35] are used as input for the analysis. Figure 6 (a) shows that for a normal distributed input force applied on the dome, the top elastomer moves uniformly downwards towards the sensing electrodes. This uniform displacement of the elastomer will result in an equal change in the capacitance of all four capacitor units. For an applied shear force on the side face of the dome, the elastomer moves downwards on one side and upwards on the other side with a symmetric displacement profile. The symmetric displacement of the elastomer under shear force validates the use of Eq. (2) and (3) for the estimation of applied shear force in the *x* and *y*-axis.

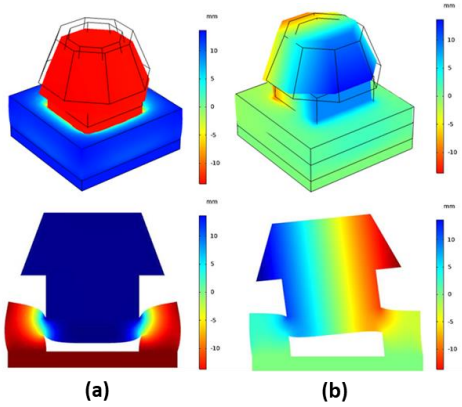

Fig. 6. Deformation profile of the sensor for an applied force in the (a) normal axis and (b) shear axis.

5. Sensor Characterization

5.1 Experimental Setup

Figure 7 shows the schematic of the experimental setup used for the characterization of the proposed capacitive tactile force sensor. The setup consists of a digital push–pull force gauge with a 50 N force range and 10 mN resolution and a tri-axis translation stage with a displacement resolution of 1 µm. The tri-axial tactile force sensor is placed on the table and the digital push–pull force gauge is attached to the translation stage in the vertical direction to measure the applied normal force in the *z*-axis. For an applied shear force, the force gauge is attached to the translation stage in the horizontal orientation to measure the applied force in *x* or *y* axis. For the normal force, the Z column of the translation stage moves downwards while for the shear force it remains stationary, and the stage table moves.

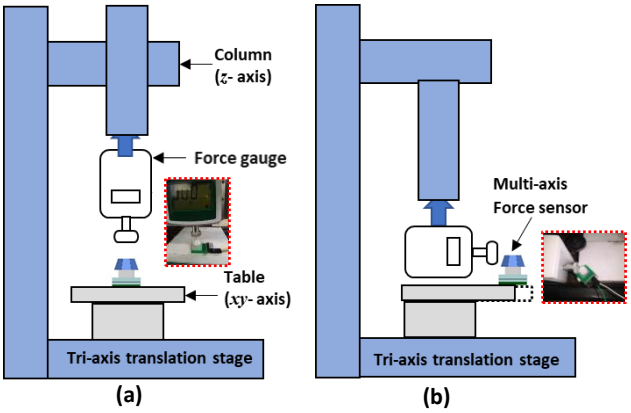

Fig. 7. Experimental setup for the sensor characterization for application of (a) normal force (b) shear force.

The capacitance change in all four capacitor units is measured using a 24-bit, 2-channel AD7746 capacitance to digital converter (CDC) with 4 fF accuracy and a minimum resolution of 4 aF. To investigate the capacitance change in all unit capacitors corresponding to an applied force, two AD 7746 CDC converters are integrated with an Arduino microcontroller unit (MCU). The MCU communicates with the AD7746 board through a multiplexer using I^2C serial communication protocol. Figure 8 shows the schematic diagram of the data acquisition system used for the testing of the sensor.

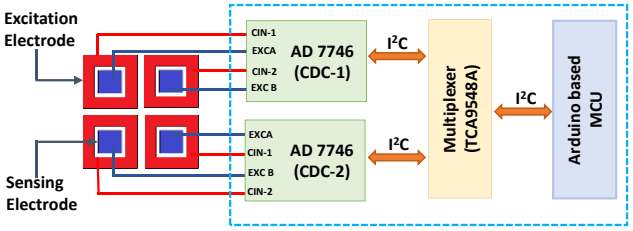

Fig. 8. Schematic diagram of the proposed sensor and the layout of the AD7746 board with the individual components.

5.2 Normal Force Characterization

Figure 9 shows the normalized change in capacitance values for the sensor in the normal direction for an input force up to 5 N. The change in capacitance of all four capacitor units is obtained using AD7746 capacitance to digital converter and normalized capacitance is plotted using Eq. 1.

For an applied force above 5N, the sensor output saturates. The measured value of the displacement in the top dielectric for an applied force of 5 N is 1.2 mm. The output saturation of the sensor for applied force above 5 N can be attributed to the fact that the initial gap or air cavity height between the capacitor units and elastomer layer is fully transversed.

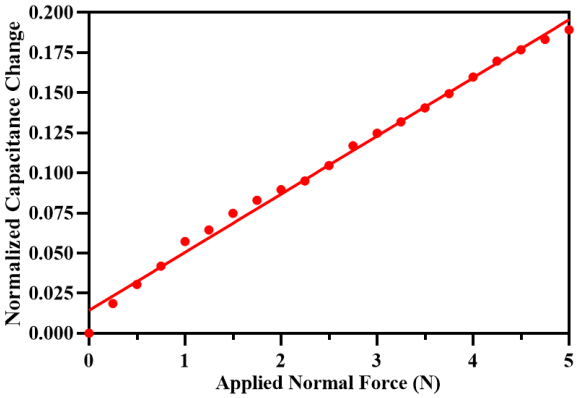

Fig. 9. Normalized capacitance changes for an applied force in the normal direction (ΔC_Z).

The dielectric constant of the Ecoflex 00-30 elastomer is 2.8 and that of air is 1. When a normal force is applied to the bump of the sensor, the air cavity size decreases which leads to a change in the effective dielectric constant which lies in the range of 1-2.8 for an applied normal force. The increase in the normalized capacitance with an increase in the applied force, shown in Fig. 9, can thus be explained by an increase in the effective dielectric constant. The normalized sensitivity of the proposed sensor obtained from Fig. 9 is 0.0378/N. This sensitivity value is better than the normal force sensitivity values of 0.0095/N and 0.0192/N reported in [29] and [33] for the fringing field based capacitive tactile force sensors.

5.3 Shear and Angular Force Characterization

As discussed in Section 2, for an input force in the shear axis (*x* and *y*-axis), the top Ecoflex 00-30 elastomer moves in such a way that the gap between the elastomer and two of the capacitor units decreases, and in other two increases. Figure 10 (a) shows the normalized capacitance change in the capacitor units for an input force in the +*x*-axis. The results show that with an increase in the input force, the normalized capacitance of capacitor units C_3, C_4 increases and that of the capacitance of C_1, C_2 decreases which can be attributed to the increases and decreases in the effective dielectric constant above the capacitor units for C_3, C_4 and C_1, C_2 respectively. The ΔC_x is the response of the sensor which is plotted by using Eq. (2) when a shear force is applied in *x*-axis.

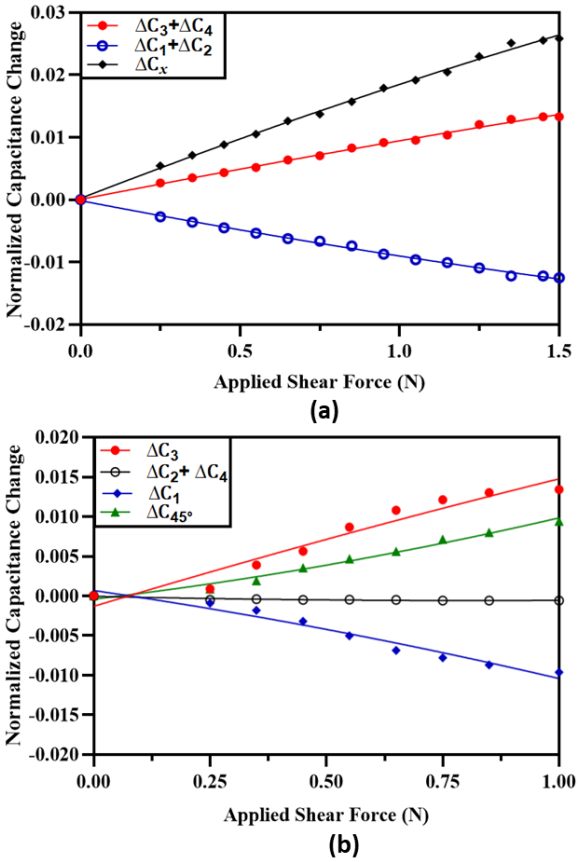

Fig. 10. Normalized capacitances change for an input force in (a) shear + x-axis (b) at an angle of 45°.

The normalized sensitivity of the sensor for a shear force in the +*x*-axis is 0.018/N for a force range of 1.5 N. Since, the sensor is symmetric in configuration, a similar response can be expected for an applied force in ± *y*-axis and -*x*-axis. As shown in Fig. 10(b), for input force at an angle of 45°, the capacitance of the C_3 increases, for the C_1 is decreases, while remains constant for C_2 and C_4 because a resultant change in the height of the air cavity on the top of capacitor units C_2 and C_4 is zero. The $\Delta C_{45°}$ is the response of the sensor plotted using Eq. (4) when an angular force is applied at a 45° angle. The normalized value of sensor sensitivity for angular force is 0.010/N for a force range of 1 N.

Figure 11 (a) shows the *x*-axis and *y*-axis output response of the sensor for an input force in the *x*-axis. The results show that for an input force in the *x*-axis, the normalized ΔC_x value changes linearly for an input force in the range of 0 to 1.5 N while there is slightly a change in the normalized ΔC_y. The maximum value of normalized ΔC_y is -0.0025 for an input force of 1.5 N which ideally should have been zero. However, for an applied force in the *y*-axis, the change in the normalized ΔC_x value is constant, as shown in Fig. 11 (b), which shows a fully decoupled output response with negligible mechanical crosstalk of the sensor for an applied shear force.

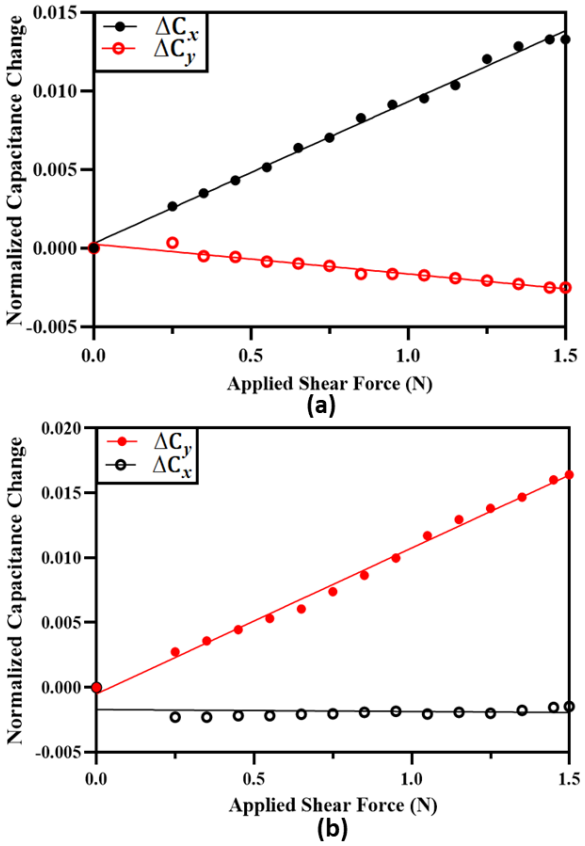

Fig. 11. Normalized capacitance changes of the sensor for an input force in the (a) x-axis (b) y-axis.

To evaluate the multi-axis tactile force sensor response in 3-dimensional space, the capacitive response of the sensor is tested by applying the angular force at angles of 45°,135°, 225°, and 315°. The normalized capacitance change plots for applied forces at different angles are shown in Fig. 12. The plots are obtained by using measured capacitance values in Eq. (4) to (7). The results show that the input angular shear force range is 0 to 1 N for all four tested angles.

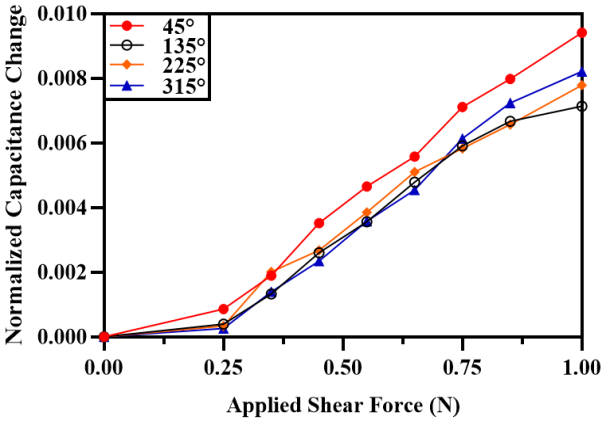

Fig. 12. The normalized capacitance change of the proposed sensor when a shear force is applied at four different angles.

The normalized capacitance change for the four angles is close to each other owing to the symmetric configuration of the stationary electrodes on the substrate. The small variations in the output can be explained by the non-uniform distribution of the top dielectric elastomer Ecoflex 00-30 and variation in the geometric dimensions of the electrodes due to manufacturing tolerances. The normalized sensitivity of the proposed tactile force sensor for angular forces at 45°,135°, 225°, and 315° is 0.0098/N, 0.0067/N, 0.0078/N, and 0.0082/N respectively for a shear force in the range of 0 to 1 N.

6. Effect of Air Cavity Height on the Sensor Output Response

To analyze the effect of the air cavity height between the stationary electrodes on the bottom substrate and top Ecoflex 00-30 elastomer layer on the sensor output response, the sensors with different air cavity heights of 2.2 mm, 1.8 mm, 1.4 mm and 1.2 mm are fabricated and tested. Figure 13 (a) shows the normalized output capacitance change for the sensors with different air cavity heights for an applied normal force. For the sensor with an air cavity height of 2.2 mm, there are three distinct regions for the output capacitance change. For an input force up to 0 to 2 N, the output is nearly zero and for input force in the range of 2 N to 5 N there is a linear increase in the output capacitance which finally saturates for input force above 5 N. For the sensor with an air cavity height of 1.8 mm, the output capacitance changes increase linearly up to 2 N at slow rate. However, for the input force in the range of 2 N to 4 N, there is a sharp increase in the output capacitance of the sensor which finally decreases for input forces above 4 N. In comparison to the sensors with air cavity heights of 2.2 mm and 1.8 mm, the sensors with air cavity heights of 1.4 mm and 1.2 mm show a smooth and linear output response for an input force in the range of 0 to 5 N. The normalized output capacitance change for the sensor with an air cavity height of 1.2 mm is slightly higher than that of the sensor with an air cavity height of 1.4 mm. Figure 13 (b) shows the output capacitance change for the sensors with different cavity heights for an input shear force in the +*x*-axis. The results show that the output capacitance change follows a similar trend for all the sensors. However, the slope and hence the sensitivity of the sensors increases with a decrease in the air cavity height. The results presented in Fig. 13 can be explained with the electric field distribution plot shown in Fig. 14. The strength of the electric field lines is higher in the vicinity of the stationary electrodes on the substrate and decreases linearly as the upwards distance increases. For the sensors with air cavity heights of 2.2 mm and 1.8 mm, it can be observed that electric field strength is initially nearly zero which explains that for an applied normal force upto 2 N the output capacitance change of these sensors is almost negligible. However, as the force

increases, the top elastomer reaches the relatively dense electric field lines and significant output capacitance change is observed. For the sensors with air cavity heights of 1.4 mm and 1.2 mm, the electric field lines are dense in 1.2 mm height then 1.4 mm height, which leads to a distinguishable capacitance change as the force is applied. These results show that for the fringe effect based capacitive force sensors, it is very important to quantify the electric field strength to obtain the air cavity height.

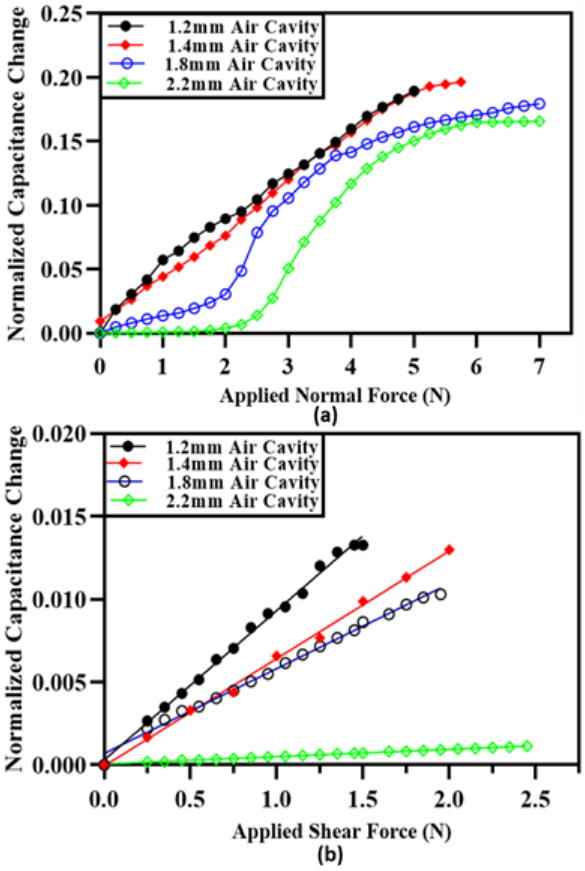

Fig. 13. Output normalized capacitance response of the sensors with different air cavity heights for an applied (a) normal force and (b) shear force.

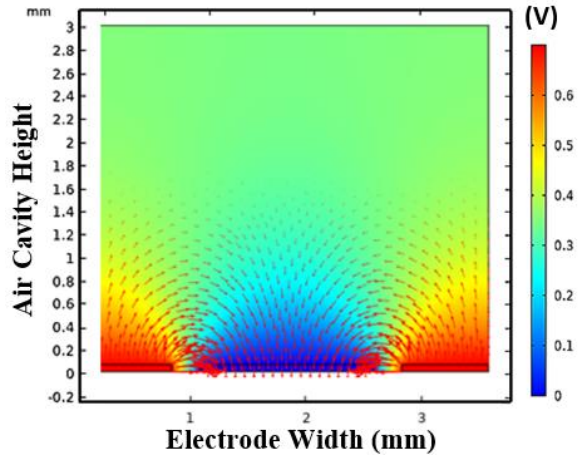

Fig. 14. Electric field lines distribution above the stationary electrodes on the substrate with respect to air cavity height.

The results in Fig. 13 (a) and (b) for the sensors with air cavity heights of 1.4 mm and 1.8 mm show that the difference in the output capacitance change between these two sensors for an applied shear force is higher in comparison to the applied normal force. This is because the elastomer layer that is used to achieve the air cavity has less stiffness when its height is 1.8 mm in comparison to 1 mm height. This leads to higher shear displacement in the case of a 1.8 mm air cavity sensor as shown in Fig. 15.

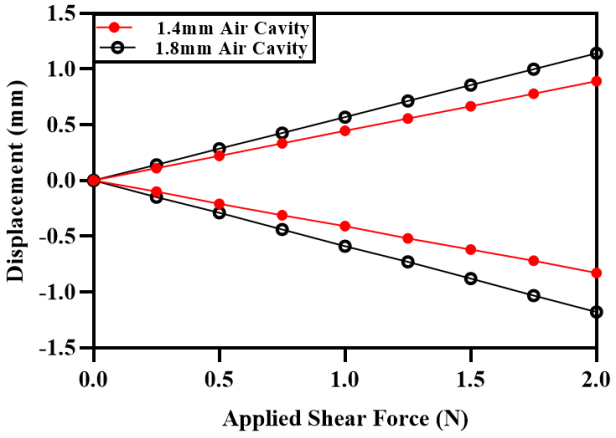

Fig. 15. The elastomer displacement profile in the ± x-axis for an applied shear force.

7. Force Estimation Based on the Measured Capacitance Change

To estimate the forces from the measured output capacitance values of the sensor under an applied force, a mathematical model is required which enables the sensor to interact in the real environment. The proposed sensor is calibrated for the full range of applied forces and second order polynomial expressions are obtained, for both the normal and shear forces, by curve fitting to obtain the expression coefficients. The final expressions for the force estimation by the measured capacitance change in the normal and shear axis are given as;

$$\Delta C_z = -0.0016F^2 + 0.0442F + 0.0079 \quad (11)$$

$$\Delta C_x = -0.0006F^2 + 0.01F + 0.0005 \quad (12)$$

Where ΔC_z is the normalized capacitance change in the normal axis, which is caused by normal force application, ΔC_X is the normalized capacitance change in the shear axis which is due to the shear force application and F is the magnitude of the applied force. Figure 16 (a) and (b) show the comparison of the actual applied force and that estimated force using the developed analytical expressions for both the normal and shear forces. The results show a close correspondence and hence validate the accurate estimation of the applied force to the sensor from the measured output capacitance change.

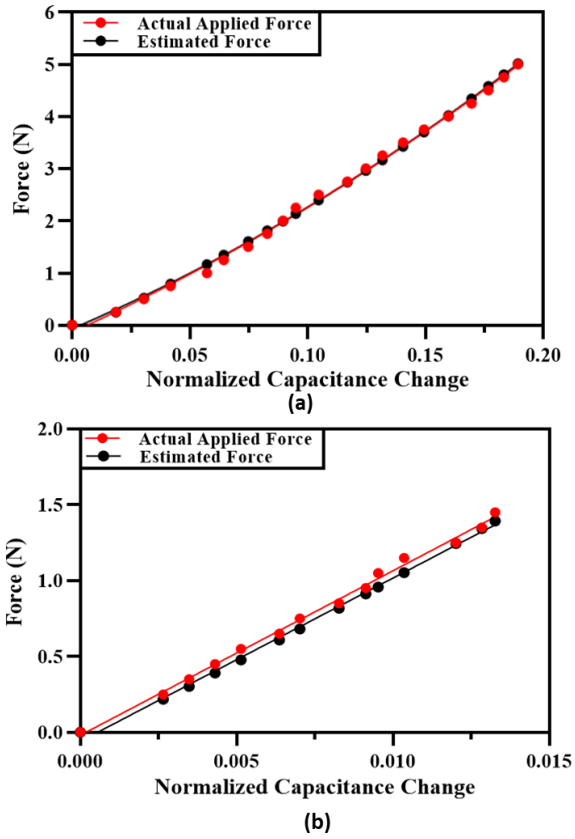

Fig. 16. Comparison of the applied force and estimated force by the measured capacitance change for (a) normal force (b) shear x-axis force.

8. Hysteresis and Repeatability Analysis

One of the important characteristics of a tactile force sensor is the consistency in the output response values for increasing and decreasing input force. The difference in the output values during the increasing and decreasing cycle of the applied force is usually dependent on the material properties of a sensor. Figure 17 shows the hysteresis plot for the proposed sensor where the normal input force is increased from 0 to 5 N and then subsequently decreased to 0 N with the step size of 0.1 N and corresponding normalized capacitance change values are plotted.

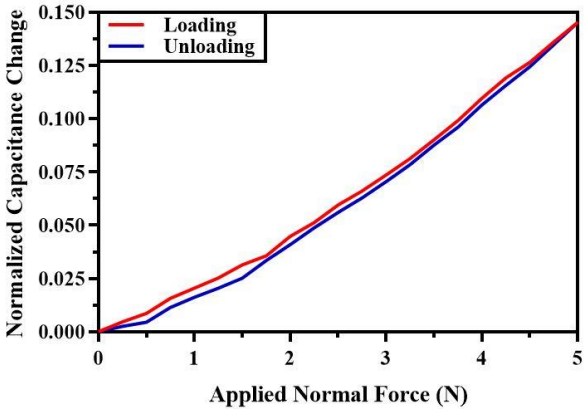

Fig. 17. Hysteresis response of the multi-axis tactile force sensor.

The difference in normalized capacitance change during the applied normal force region of 0 - 1.75 N is due to stress relaxing behaviour of elastomer Ecoflex 00-30. The results show that the difference in the capacitance change values during increasing and decreasing input force with a percentage difference of only 2.64 % is obtained based on the measured data.

The repeatability of a tactile sensor is an important parameter for use in the robotics surgical system. The repeatability analysis of the proposed multi-axis tactile force sensor is performed for five loading cycles once a day for five consecutive days. The capacitive response of the multi-axis tactile force sensor is analyzed for 5 N force in normal direction (z-axis). Figure 18 shows the repeatability test results of the proposed sensor with the mean (line) of five values and negligible standard deviation (error bar) corresponding to an applied normal force. The sensor shows good signal stability by exhibiting the repeatability error of 4.15 %.

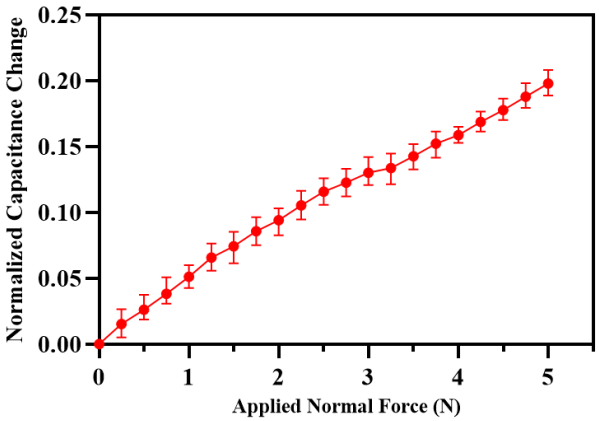

Fig. 18. The capacitive response of the proposed multi-axis tactile force sensor for the five loading cycles.

9. Dynamic Output Response

The output capacitance response is obtained by using four and six rising and falling force ramps for the 2 Hz and 3 Hz input forces respectively as shown in Fig. 19. The results show that the output capacitance change follows the input force. The slight drift in the input force amplitude for different cycles can be attributed to the alignment errors of the tri-axis translation stage. The values of the normalized capacitance change for both the 2 Hz and 3 Hz input forces of 1 N are close to the static input force with a value equivalent to 0.022. The minor delay in the output capacitance for an input dynamic force can be attributed to the viscoelastic behavior of the elastomer. The accurate response of the sensor for an input frequency up to 3 Hz shows that the proposed sensor can be used for laparoscopic MIRS applications where the grasping frequency is usually below 3 Hz [36, 37]. The sensor bandwidth is dependent on the sampling frequency of the digital capacitance to voltage conversion IC used in the experimental characterization which is 90.9 Hz. In the robotic surgical

systems, the desired bandwidth is generally dictated by the application which may be as high as 500 Hz for the force feedback [38]. However, due to experimental setup limitations, we were unable to obtain the dynamic response of the sensor for input forces with input frequency above 3 Hz.

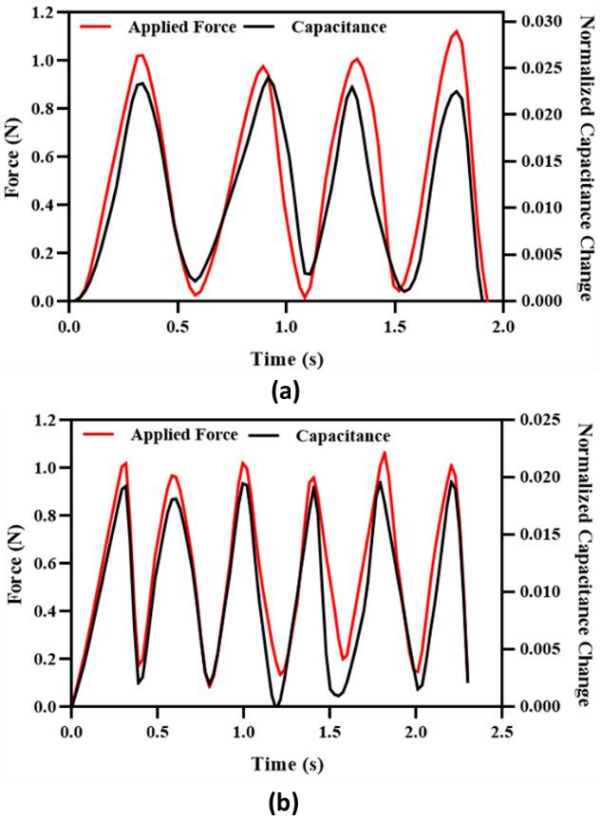

Fig. 19. Normalized output capacitance of the sensor for an input normal force applied at (a) 2 Hz and (b) 3 Hz.

10. Stability Analysis

To analyze the effect of the variation in the atmospheric temperature on the output response of the sensor, the sensor is placed inside an acrylic chamber and temperature is increased by using a heat gun. Actual temperature inside the acrylic chamber is measured using a standard digital thermometer. Figure 20 (a) shows the experimental setup for the analysis of environmental temperature variations on the sensor. The sensor was tested in the temperature changing environment from 25 °C to 40 °C under no loading condition. The results in Fig. 20 (b) show that with an increase in the environment temperature the nominal capacitance of the sensor increases and the variation in the nominal capacitance value is nearly 2.5 % at 40 °C with respect to 25 °C. The temperature sensitivity of the proposed sensor is 4.4 fF/°C which can be further minimized by implementing temperature error compensation techniques.

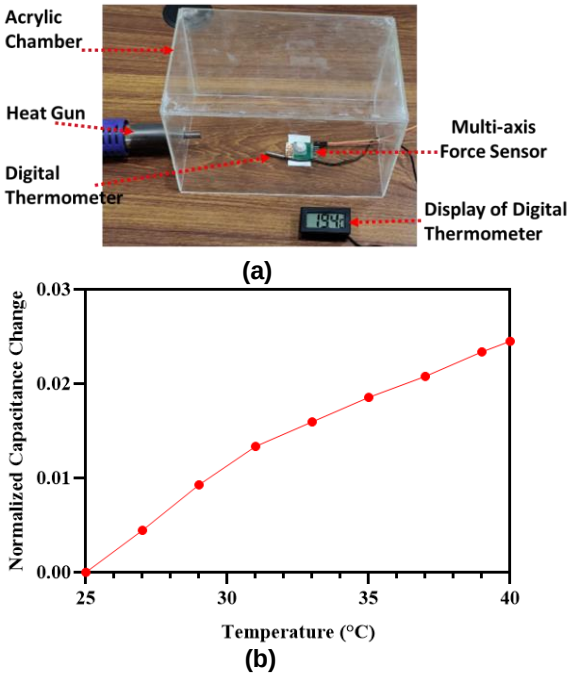

Fig. 20. Effect of environmental temperature variations on the sensor (a) experimental setup (b) normalized capacitance change for temperature in the range of 25 °C to 40 °C.

In addition to the temperature variations, the effect of the surrounding interference on the out response of the sensor is evaluated by hovering the human finger from 0 cm to 20 cm above the sensor and analyzing the nominal output capacitance under no load condition. Moreover, to compare the effect of the sensor shielding, output response of both shielded and unshielded sensor is evaluated. The sensor is shielded by integrating a flexible metal coated sheet below FR4 substrate and between the elastomer and elastomer dome and connecting to the ground. The flexible metal sheet is achieved using an inkjet printing technique by printing a conductive silver nanoparticles-based ink on a flexible Polyethylene terephthalate (PET) sheet of 0.135 mm thickness. Figure 21 shows the normalized capacitance of both shielded and unshielded sensors with varying human finger height above the sensor. The results show that for the unshielded sensor, the nominal output capacitance of the sensor decreases to 1.5 % of its original value when the human finger distance is 2 cm above the sensor. By increasing the finger distance to 12 cm above the sensor, the output capacitance approaches the nominal capacitance value. For the shielded sensor, the output capacitance decreases to 1 % of its original value and approaches the nominal value when human finger is at 8 cm above the sensor. These results show that shielding the proposed tactile force sensor, can further increase the robustness of the sensor to the surrounding environment interference.

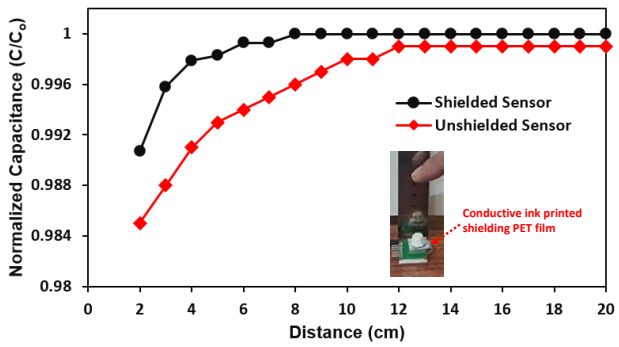

Fig. 21. Effect of varying human finger distance from both the shielded and unshielded

11. Conclusion

A fringing field effect-based capacitive tactile force sensor is presented that can measure and decouple normal, shear ±*xy*-axis and angular shear forces. An analytical model is presented that estimates the nominal capacitance value of the stationary fringing field electrodes with respect to the geometric dimensions of the electrodes and air cavity height between electrodes and the top elastomer. The sensor is low-cost that is fabricated using rapid prototyping techniques. The geometric design and configuration of the stationary fringing field electrodes in the sensor allowed to attain higher sensitivity and linearity in comparison to the fringing field effect-based tactile force sensors presented in the literature. The normalized capacitance sensitivity for normal and shear axis is 0.0378/N and 0.018/N respectively while for the shear angular force it is 0.010/N. The sensor is tested for its repeatability and hysteresis error which showed a reliable operation of the sensor. The frequency response of the sensor showed that proposed sensor can be used for the measurement of dynamic input forces up to 3 Hz frequency. The demonstrated force measurement ranges, high sensitivity with repeatability and flexible contact surface allow the potential application of the proposed fringing field effect-based tactile force sensor in MIRS for the force feedback from the surgical instrument to the surgeon. The possible future improvement for the proposed sensor is to achieve better thermal stability and use of biocompatibile flexibilie materials for integration at the end of surgical tool in MIRS.

Acknowledgments

This work was supported by the Higher Education Commission (HEC), Pakistan and the British Council UK within the framework of the Innovative and Collaborative Research Partnerships Grants (ICRG) program under the project. No. ICRG-147.

References

[1] Pohtongkam, Somchai, and Jakkree Srinonchat. "Tactile Object Recognition for Humanoid Robots Using New Designed Piezoresistive Tactile Sensor and DCNN." *Sensors* 21, no. 18 (2021): 6024.

[2] Jaschinski, Thomas, Christoph G. Mosch, Michaela Eikermann, Edmund AM Neugebauer, and Stefan Sauerland. "Laparoscopic versus open surgery for suspected appendicitis." *Cochrane Database of Systematic Reviews* 11

[3] Vyas, Dinesh, and Sean Cronin. "Peer review and surgical innovation: robotic surgery and its hurdles." *American journal of robotic surgery* 2, no.

[4] Saccomandi, Paola, Emiliano Schena, Calogero Maria Oddo, Loredana Zollo, Sergio Silvestri, and Eugenio Guglielmelli. "Microfabricated tactile sensors for biomedical applications: a review." *Biosensors* 4, no. 4 (2014):

[5] Yousef, Hanna, Mehdi Boukallel, and Kaspar Althoefer. "Tactile sensing for dexterous in-hand manipulation in robotics—A review." *Sensors and Actuators A: physical* 167, no. 2 (2011): 171-187.

[6] Taniguchi, Tadahiro, Daichi Mochihashi, Takayuki Nagai, Satoru Uchida, Naoya Inoue, Ichiro Kobayashi, Tomoaki Nakamura, Yoshinobu Hagiwara, Naoto Iwahashi, and Tetsunari Inamura. "Survey on frontiers of language and robotics." *Advanced Robotics* 33, no. 15-16 (2019): 700-730.

[7] Wang, Xin, John Sparkman, and Jihua Gou. "Strain sensing of printed carbon nanotube sensors on polyurethane substrate with spray deposition modeling." *Composites Communications* 3 (2017): 1-6.

[8] Mukai, Toshiharu, Masaki Onishi, Tadashi Odashima, Shinya Hirano, and Zhiwei Luo. "Development of the tactile sensor system of a human-interactive robot "RI-MAN"." *IEEE Transactions on robotics* 24, no. 2

[9] Karmakar, Rajat Subhra, Chia-Pei Chu, Ying-Chih Liao, and Yen-Wen Lu. "PVA tactile sensors based on Electrical Contact Resistance (ECR) change mechanism for subtle pressure detection." *Sensors and Actuators A:*

[10] Dargahi, J. "A piezoelectric tactile sensor with three sensing elements for robotic, endoscopic and prosthetic applications." *Sensors and Actuators A: Physical* 80, no. 1 (2000): 23-30.

[11] Chen, Songyue, Cheng Bai, Chenying Zhang, Da Geng, Ruiliang Liu, Yu Xie, and Wei Zhou. "Flexible piezoresistive three-dimensional force sensor based on interlocked structures." *Sensors and Actuators A: Physical* 330 (2021): 112857.

[12] Takahashi, Hidetoshi, Akihito Nakai, Nguyen Thanh-Vinh, Kiyoshi Matsumoto, and Isao Shimoyama. "A triaxial tactile sensor without crosstalk using pairs of piezoresistive beams with sidewall doping." *Sensors and Actuators A: Physical* 199 (2013): 43-48.

[13] Giesberts, Robert Bram, Victor IJzebrand Sluiter, and Gijsbertus Jacob Verkerke. "Design and test of a new inductive force sensor." *Sensors* 18, no. 7 (2018): 2079.

[14] Wang, Lefan, Dominic Jones, Graham J. Chapman, Heidi J. Siddle, David A. Russell, Ali Alazmani, and Peter Culmer. "An inductive force sensor for in-shoe plantar normal and shear load measurement." *IEEE Sensors Journal* 20, no. 22 (2020): 13318-13331.

[15] Chatzipirpiridis, George, Pascal Erne, Olgaç Ergeneman, Salvador Pané, and Bradley J. Nelson. "A magnetic force sensor on a catheter tip for minimally invasive surgery." In *2015 37th Annual International Conference of the IEEE Engineering in Medicine and Biology Society (EMBC)*, pp. 7970-7973. IEEE, 2015.

[16] Rehan, Muhammad, Muhammad Mubasher Saleem, Mohsin Islam Tiwana, Rana Iqtidar Shakoor, and Rebecca Cheung. "A Soft Multi-Axis High Force Range Magnetic Tactile Sensor for Force Feedback in Robotic Surgical Systems." *Sensors* 22, no. 9 (2022): 3500.

[17] Zhu, Yinlong, Xin Chen, Kaimei Chu, Xu Wang, Zhiqiang Hu, and Haijun Su. "Carbon Black/PDMS Based Flexible Capacitive Tactile Sensor for Multi-Directional Force Sensing." *Sensors* 22, no. 2 (2022): 628.

[18] Kim, Hong-Ki, Seunggun Lee, and Kwang-Seok Yun. "Capacitive tactile sensor array for touch screen application." *Sensors and Actuators A: Physical* 165, no. 1 (2011): 2-7.

[19] Lee, Chengkuo, Toshihiro Itoh, and Tadatomo Suga. "Micromachined piezoelectric force sensors based on PZT thin films." *IEEE transactions on ultrasonics, ferroelectrics, and frequency control* 43, no. 4 (1996): 553-559.

[20] Li, Ming, Wei Cheng, Jiangpan Chen, Ruili Xie, and Xiongfei Li. "A high performance piezoelectric sensor for dynamic force monitoring of landslide." *Sensors* 17, no. 2 (2017): 394.

[21] Cataldi, Pietro, Dimitrios G. Papageorgiou, Gergo Pinter, Andrey V. Kretinin, William W. Sampson, Robert J. Young, Mark Bissett, and Ian A. Kinloch. "Graphene–polyurethane coatings for deformable conductors and electromagnetic interference shielding." *Advanced Electronic Materials* 6, no. 9 (2020): 2000429.

[22] Xie, Cheng, Jia Li, and Weibing Wang. "A package for piezoresistive pressure sensors with embedded built-in self-test function based on bimetallic actuator." *Sensors and Actuators A: Physical* (2022): 113817.

[23] Valdastri, P., S. Roccella, L. Beccai, E. Cattin, A. Menciassi, M. C. Carrozza, and P. Dario. "Characterization of a novel hybrid silicon three-axial force sensor." *Sensors and Actuators A: Physical* 123 (2005): 249-257.

[24] Tumanski, Slawomir. "Induction coil sensors—A review." *Measurement Science and Technology* 18, no. 3 (2007): R31.

[25] Lemarquand, V. "A new bi-directional inductive force sensor." *IEEE transactions on magnetics* 34, no. 4 (1998): 1333-1335.

[26] Liang, Qiaokang, Kunlin Zou, Jianyong Long, Jing Jin, Dan Zhang, Gianmarc Coppola, Wei Sun, Yaonan Wang, and Yunjian Ge. "Multi-component FBG-based force sensing systems by comparison with other sensing technologies: A review." *IEEE sensors journal* 18, no. 18 (2018):

[27] Sun, Yu, Bradley J. Nelson, David P. Potasek, and Eniko Enikov. "A bulk microfabricated multi-axis capacitive cellular force sensor using transverse comb drives." *Journal of Micromechanics and Microengineering* 12, no. 6 (2002): 832.

[28] Lee, Hyung-Kew, Jaehoon Chung, Sun-Il Chang, and Euisik Yoon. "Normal and shear force measurement using a flexible polymer tactile sensor with embedded multiple capacitors." *Journal of Microelectromechanical Systems* 17, no. 4 (2008): 934-942.

[29] Huang, Ying, Haitao Yuan, Wenqing Kan, Xiaohui Guo, Caixia Liu, and Ping Liu. "A flexible three-axial capacitive tactile sensor with multilayered dielectric for artificial skin applications." *Microsystem Technologies* 23, no. 6 (2017): 1847-1852.

[30] Kang, Subin, Jaehong Lee, Sanggeun Lee, SeulGee Kim, Jae-Kang Kim, Hassan Algadi, Saleh Al-Sayari, Dae-Eun Kim, DaeEun Kim, and Taeyoon Lee. "Highly sensitive pressure sensor based on bioinspired porous structure for real-time tactile sensing." *Advanced Electronic Materials* 2, no. 12 (2016): 1600356.

[31] Liu, G. D., C. H. Wang, Z. L. Jia, and K. X. Wang. "An Integrative 3D printing method for rapid additive manufacturing of a capacitive force sensor." *Journal of Micromechanics and Microengineering* 31, no. 6 (2021):

[32] Fernandes, Jayer, Jiangang Chen, and Hongrui Jiang. "Three-Axis Capacitive Sensor Arrays for Local and Global Shear Force Detection." *Journal of Microelectromechanical Systems* 30, no. 5 (2021): 799-813.

[33] Sun, Ying, Fei Liu, Zipeng Yuan, Wenmei Huang, and Bowen Wang. "A novel three-axial force tactile sensor based on the fringing effect of electric field." *IEEE Transactions on Magnetics* 55, no. 9 (2019): 1-5.

[34] Li, Nan, Haiye Zhu, Wenyu Wang, and Yu Gong. "Parallel double-plate capacitive proximity sensor modelling based on effective theory." *Aip Advances* 4, no. 2 (2014): 027119.

[35] Vaicekauskaite, Justina, Piotr Mazurek, Sindhu Vudayagiri, and Anne Ladegaard Skov. "Mapping the mechanical and electrical properties of commercial silicone elastomer formulations for stretchable transducers." *Journal of Materials Chemistry C* 8, no. 4 (2020): 1273-1279.

[36] Sarmah, Apu, and U. D. Gulhane. "Surgical robot teleoperated laparoscopic grasper with haptics feedback system." In INTERACT-2010, pp. 288-291. IEEE, 2010.

[37] Ly, Hiep Hoang, et al. "Grasper having tactile sensing function using acoustic reflection for laparoscopic surgery." International Journal of Computer Assisted Radiology and Surgery 12.8 (2017): 1333-1343.

[38] Jones, D., Wang, H., Alazmani, A. and Culmer. “A soft multi-axial force sensor to assess tissue properties in realtime.” IEEE/RSJ International Conference on Intelligent Robots and Systems (2017): 5738-5743.